J. Fluid Mech. (1984), *vol.* 138, *pp.* 379–404
Printed in Great Britain

Secondary flow and turbulence in a cone-and-plate device

By H. P. SDOUGOS, S. R. BUSSOLARI AND C. F. DEWEY
Fluid Mechanics Laboratory, Massachusetts Institute of Technology, Cambridge, Massachusetts

(Received 22 October 1982 and in revised form 1 September 1983)

The flow between a shallow rotating cone and a stationary plate has been investigated using flow visualization, hot-film heat-transfer probes, and measurements of the torque required to rotate the cone against the retardation of the viscous fluid that fills the device. Theory appropriate to these experiments is also presented.

An expansion of the Navier–Stokes equations is performed for small values of the single parameter $\tilde{R} = r^2\omega\alpha^2/12\nu$. (Here r is the local radius, ω the angular velocity of the cone, $\alpha(\ll 1)$ is the angle between the cone and plate, and ν is the fluid kinematic viscosity.) The measurements at low rotational speeds describe a simple linear velocity profile as predicted for the laminar flow of a Newtonian fluid. At larger rotational speeds, strong secondary flows are observed. There is agreement between the laminar theory and the measured streamline angles and shear stresses for values of $\tilde{R} < 0.5$. Turbulence is observed for $\tilde{R} \gtrsim 4$.

1. Introduction

This paper describes the secondary flow and turbulence in the fluid between a rotating cone and a stationary flat plate. This flow has been of substantial interest in the past primarily because it is a geometry used frequently in commercial viscometers. The motivation of the present research, however, was to develop an apparatus with a well-characterized flow in which damage to living cells by fluid shear stress could be investigated (Dewey *et al.* 1981).

This Introduction provides a physical description of the various forces acting on the fluid and an explicit statement of the flow pattern in the limit of very small cone angle and slow rotation. A single flow parameter that characterizes the flow is defined and a summary of other relevant investigations is also presented. The asymptotic expansion method used to obtain a theoretical description of laminar secondary flow in the device is described in §2. The experimental apparatus is described in §3, and results are presented and discussed in §4.

1.1. *Introductory description of the flow*

Cone-and-plate viscometers are conventionally operated under conditions where negligible secondary flow exists. In this case, flow streamlines are concentric circles. Both the gap width $h(r)$ and the azimuthal cone surface velocity $v_0(r)$ increase linearly with radius, so that the shear rate

$$\frac{\partial v}{\partial z} = \frac{v_0}{h}$$

is identical at every point within the fluid as well as on the cone and plate surfaces.

The operating requirements for testing living cells (Bussolari, Dewey & Gimbrone,

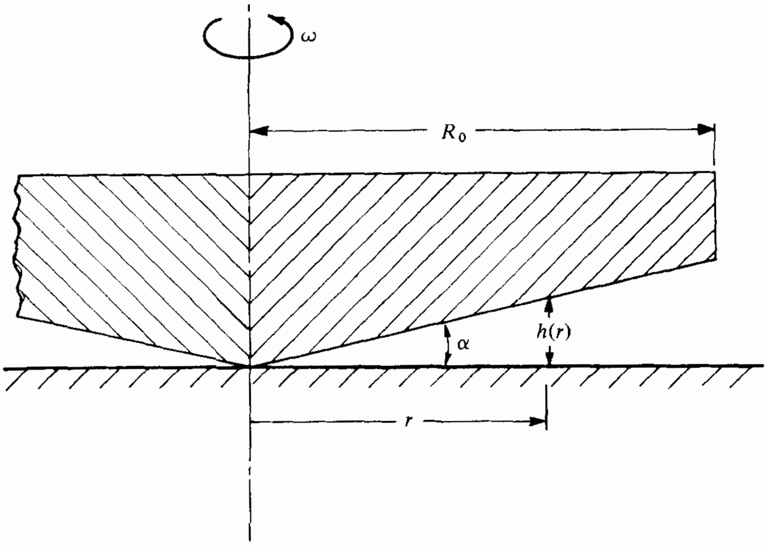

FIGURE 1. Geometry of the cone-and-plate apparatus defining the nomenclature used.

1982) vary considerably from those that apply to normal viscometers. In particular, a desirable attribute would be the ability to produce both laminar and turbulent flow in a single device while having the same time-average shear stress at the surface of the plate. It is demonstrated in §5 that this is possible.

The variables governing the flow are summarized in figure 1. In the limit of low rotational speed and small cone angle, the streamlines are concentric circles and, with a Newtonian fluid, the surface shear stress is

$$\tau = \mu \frac{\partial v}{\partial z} = \mu \frac{v_0}{h} = \mu \frac{\omega r}{r \tan \alpha}, \tag{1}$$

where μ is the viscosity of the fluid and z is the coordinate normal to the plate. With a sufficiently small cone angle, $\tan \alpha$ may be replaced by α, and the shear stress can be expressed as

$$\tau = \mu\omega/\alpha, \tag{2}$$

where ω is the angular velocity of the cone. The surface shear stress is thus constant. This situation is termed *primary flow*.

As the angle α and rotational rate ω increase, the fluid near the cone experiences an increasing centrifugal force that promotes radial fluid motion towards the periphery of the device. The relative magnitudes of centrifugal and viscous forces are measured by a parameter termed $\tilde{R}$. This parameter represents the ratio of the characteristic centrifugal force to the characteristic viscous force acting on the fluid at any radius from the centre of the cone. The characteristic centrifugal force per unit fluid volume can be expressed as

$$\frac{\rho v_0^2}{r} = \rho r \omega^2, \tag{3}$$

where ρ is the fluid density. The corresponding viscous force is τ/h, or $\mu v_0/h^2$. The ratio of these two terms is

$$\frac{\text{centrifugal force}}{\text{viscous force}} = \frac{r^2 \omega \alpha^2}{\nu}, \tag{4}$$

where ν is the fluid kinematic viscosity μ/ρ. In the Appendix it is demonstrated that an ordering of all variables such that the non-dimensional equations contain terms of order unity leads to a factor of 12 in the denominator of the parameter $\tilde{R}$. Henceforth the single parameter used to describe the flow is

$$\tilde{R} = \frac{r^2\omega\alpha^2}{12\nu}, \tag{5}$$

and thus the significant physical variables for cone–plate flow are ρ, μ, α, r, ω.

1.2. *Previous descriptions of cone-and-plate flow*

As has already been noted, by far the most common use for the rotating cone-and-plate configuration has been in viscometry. This device was first introduced by Mooney & Ewart (1934), and provides viscosity data for fluids with various stress–strain relations. The advantage of the cone-and-plate configuration over other viscometers is that shear stress and shear rate are constant throughout the fluid sample provided that the gap angle α (and hence $\tilde{R}$) is kept sufficiently small. Typical commercial devices employ a cone angle of 0.3° and a radius of approximately 2–3 cm. Most previous theoretical treatments of the cone-and-plate configuration describe flows dominated by primary flow (Walters 1975; Coleman, Markovitz & Noll 1966; Walters & Waters 1966).

Secondary-flow phenomena in a cone-and-plate device were apparently first observed by Cox (1962) using dye-visualization techniques. Several analyses and experiments appeared contemporaneously with the observations of Cox: the experiment and analysis of Miller & Hoppmann (1963), where large cone angles were used; the analysis of Slattery (1961), which clearly described the conditions under which secondary flow could be neglected; and the experiment and detailed theory of Pelech & Shapiro (1964), which treated the related problem of flow between a spinning flexible disk and a stationary flat plate.

Pelech & Shapiro were the first to clearly identify the parameter governing secondary fluid motion in this type of flow geometry as being the ratio of the fluid centrifugal forces to viscous forces. They derived a parameter for their spinning-flexible-disk problem that is equivalent to the parameter $\tilde{R}$ used here. Walters & Waters (1966) used the dimensionless parameter $L = \omega b^2/\nu$ in their analysis, where ω is a typical angular velocity and b is a typical length such as the cone outer radius. The parameter L is equivalent to $\tilde{R}$, except that the term α^2 is omitted and the length parameter b is typical of the device as a whole and does not refer to the local radius of the point under investigation. Thus L does not refer to the local ratio of viscous to centrifugal forces at any position within the apparatus.

Walters & Waters expanded the equations of motion for small values of the parameter L and solved the resulting equations numerically. Two years later, Cheng (1968) published the first systematic data describing secondary flow. He measured the torque produced in a cone-and-plate viscometer and compared his results with the predictions of Walters & Waters, finding good agreement. The comparison required two independent quantities, the parameter L and the cone angle α. An attempt by King & Waters (1970) to extend this analysis to terms of higher order in the parameter L produced only marginal improvement in the agreement with experimental data in the range where strong secondary flow occurred.

Savins & Metzner (1970) developed a solution for the secondary flow in a cone-and-plate device by using the primary flow to establish the pressure field; a subsequent calculation yielded the radial component of velocity. Several of the present results, obtained by systematic expansion of the governing equations in terms of the parameter $\tilde{R}$, are identical with those found by Savins & Metzner (1970).

Turian (1972) used a two-parameter expansion method to compute secondary flow. His parameters were, in the present nomenclature, equivalent to L and α. He expanded the governing equations in terms of α and $L\alpha^2$ with the assumption that the shear stress on the cone and plate must be identical at each radial position within the device. The present analysis shows that this is incorrect. Heuser & Krause (1979) arrived at results similar to those of Turian, and extended the asymptotic equations to encompass the region near the edge of the cone. They represent the outer boundary by a liquid free surface. Only a perturbation solution to this outer flow is attempted.

The most complete theoretical study of this geometry to date was completed by Fewell & Hellums (1977). Secondary flow was computed using finite-difference numerical techniques. Again, two parameters equivalent to L and α were used. One advantage of the finite-difference solutions (and this also holds for the earlier numerical results of Walters & Waters 1966) is that the details of the flow are specified everywhere within the cone–plate space. In contrast with the solutions of Savins & Metzner, Turian, Pelech & Shapiro and the present calculations, Fewell & Hellums obtain results that can be used to predict the extent to which the flow is modified by the boundary conditions at the outer edge of the cone.

2. Theoretical description of flow in a cone-and-plate device

This section presents a solution of the equation of motion for the flow of a Newtonian liquid between a shallow rotating cone and a flat plate where the angle α (figure 1) is typically of the order of 0.08 rad (5°) or less. For such small angles, the ratio of the velocity w normal to the plate to the radial velocity u will be of order α:

$$\frac{w}{u} \sim \alpha \ll 1. \tag{6}$$

Similarly the velocity gradients normal to the plate (the z-direction) are always large compared with those in the radial (r) direction. Furthermore, the flow is taken to be rotationally symmetric about the cone axis so that all θ-direction gradients are identically zero. Thus

$$\frac{\partial}{\partial r} \ll \frac{\partial}{\partial z}, \quad w \ll (u, v), \quad \frac{\partial}{\partial \theta} = 0. \tag{7}$$

With these simplifications, the Navier–Stokes equations in cylindrical coordinates reduce to the following form:

$$r\text{-momentum} \quad -\frac{v^2}{r} = -\frac{1}{\rho}\frac{\partial p}{\partial r} + \nu\frac{\partial^2 u}{\partial z^2}, \tag{8}$$

$$\theta\text{-momentum} \quad u\frac{\partial v}{\partial r} + w\frac{\partial v}{\partial z} = \nu\frac{\partial^2 v}{\partial z^2}, \tag{9}$$

$$z\text{-momentum} \quad 0 = -\frac{1}{\rho}\frac{\partial p}{\partial z} + \nu\frac{\partial^2 w}{\partial z^2}, \tag{10}$$

$$\text{continuity} \quad \frac{\partial u}{\partial r} + \frac{u}{r} + \frac{\partial w}{\partial z} = 0. \tag{11}$$

The coordinate directions (r, θ, z) and corresponding velocities (u, v, w) are defined in figure 1. The fluid density is ρ and the kinematic viscosity is ν. An additional approximation based on $\alpha \ll 1$ is

$$\tan\alpha \approx \alpha. \tag{12}$$

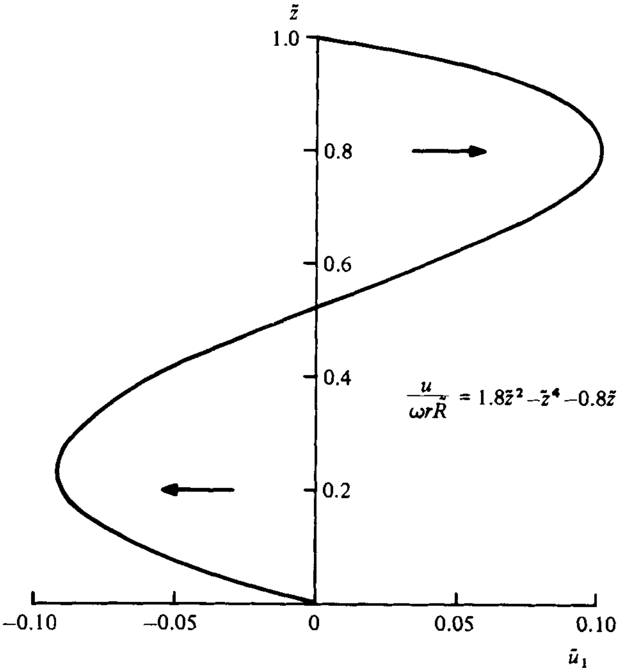

FIGURE 2. Normalized secondary-flow velocity profile $\tilde{u}_1(z)$. This is the first-order term of the radial velocity component (17).

The reduction of the Navier–Stokes equations through order-of-magnitude estimates follows directly from the analogous case of two nearly parallel spinning disks (Pelech & Shapiro 1964). The resulting equations have the character of a lubrication problem and, consistent with that analogy, it may be demonstrated, using (8)–(11), that

$$\frac{\partial p}{\partial z} \ll \frac{\partial p}{\partial r}, \quad \text{i.e.} \quad p = p(r) \text{ only}. \tag{13}$$

The boundary conditions associated with this geometry are that the fluid is in intimate contact with the rotating cone and the stationary plate. The approximations inherent in our analysis neglect edge effects at the outer rim of the cone. Clearly, this approximation will fail within several gap heights of the cone edge, but predictions of the fluid behaviour in the interior of the device should not be affected.

Solution of (8)–(11) has been obtained by the method of asymptotic expansion and is presented in the Appendix. The small parameter used in this expansion is

$$\tilde{R} \equiv \frac{r^2\omega\alpha^2}{12\nu}. \tag{14}$$

This parameter is a measure of the ratio of the centrifugal to viscous forces acting on the moving fluid. The fluid adjacent to the rotating cone experiences a centrifugal force which causes a flow in the radial direction. There is a corresponding radial flow in the opposite direction in the fluid close to the stationary plate. The normalized secondary-flow velocity profile is sketched in figure 2. When $\tilde{R} \rightarrow 0$ the centrifugal forces become small and the radial flow velocity is zero everywhere. In this limit, viscous forces dominate and (9) becomes

$$\frac{\partial^2 v}{\partial z^2} = 0, \quad \text{i.e.} \quad v(r, z) = \frac{\omega z}{\alpha}. \tag{15}$$

The viscous wall shear stress τ_w is then uniform over the whole plate surface:

$$\tau_w = \mu \left.\frac{\partial v}{\partial z}\right|_{z=0} = \frac{\mu\omega}{\alpha}. \tag{16}$$

This result is termed *primary flow*. Fluid streamlines are concentric circles about the cone apex. As $\tilde{R}$ becomes larger, centrifugal forces become significant and *secondary flow* develops.

For small values of $\tilde{R}$ (8)–(11) may be expanded in ascending powers of $\tilde{R}$ by using the following scheme:

$$u = \omega r[\tilde{u}_0 + \tilde{R}\tilde{u}_1 + \tilde{R}^2\tilde{u}_2 + \dots], \tag{17}$$

$$v = \omega r[\tilde{v}_0 + \tilde{R}\tilde{v}_1 + \tilde{R}^2\tilde{v}_2 + \dots], \tag{18}$$

$$w = \omega r\alpha[\tilde{w}_0 + \tilde{R}\tilde{w}_1 + \tilde{R}^2\tilde{w}_2 + \dots], \tag{19}$$

where the non-dimensionalized velocities are designated by a tilde. All non-dimensionalized velocities are of order unity, and it is shown in the Appendix that the terms $\tilde{u}_0$, $\tilde{w}_0$, $\tilde{v}_1$, $\tilde{u}_2$ and $\tilde{w}_2$ are identically zero. The factor α appearing in front of the brackets in (19) is a consequence of the fact that the ratio of w to u is of order α (see (6)).

The solution, the details of which are presented in the Appendix, has been carried out to second-order terms in $\tilde{R}$. The following results are obtained:

$$\tilde{v}_0 = \tilde{z}, \tag{20}$$

$$\tilde{u}_1 = 1.8\tilde{z}^2 - \tilde{z}^4 - 0.8\tilde{z}, \tag{21}$$

$$\tilde{w}_1 = 1.2(\tilde{z}^2 - \tilde{z}^3), \tag{22}$$

$$\tilde{v}_2 = \tfrac{1}{175}(-83\tilde{z} + 70\tilde{z}^4 + 63\tilde{z}^5 - 50\tilde{z}^7). \tag{23}$$

The parameter $\tilde{z}$ is the non-dimensional distance $z/\alpha r$ between the plate ($\tilde{z} = 0$) and the cone ($\tilde{z} = 1$).

In the presence of secondary flow, the fluid streamlines are no longer concentric circles and the local fluid velocity vector forms an angle ϕ with the azimuthal direction (figure 4). This angle is defined by

$$\tan\phi = \frac{u}{v}. \tag{24}$$

At the plate surface ($\tilde{z} = 0$) for small $\tilde{R}$

$$\phi = \tan^{-1}[-0.8\tilde{R} + O(\tilde{R}^3)]. \tag{25}$$

This prediction is compared with experimental results in §4.

The shear stresses $\tau_{r\theta}$ on the cone and the plate can also be expressed analytically from the theory. By differentiating (23) with respect to distance normal to the plate and evaluating the resulting expression at $\tilde{z} = 0$ and $\tilde{z} = 1$, the following relations for $\tau_{r\theta}$ are obtained:

$$\text{plate} \quad \tau_{r\theta} = \frac{\mu\omega}{\alpha}(1 - 0.4743\tilde{R}^2 + \dots), \tag{26}$$

$$\text{cone} \quad \tau_{r\theta} = \frac{\mu\omega}{\alpha}(1 + 0.9257\tilde{R}^2 + \dots). \tag{27}$$

The flow at any radius from the cone apex is considered to be a function of the local value of $\tilde{R}$; hence there is no requirement that the shear stresses on the cone and plate at that location be equal. The two expressions (26) and (27) for azimuthal shear stress on the cone and plate surfaces are compared with experimental measurements and numerical solutions of the equations of motion in §4.

3. Experimental methods

The experiments reported in this paper were chosen to illustrate different aspects of the secondary flow and turbulence that occur in the cone-and-plate geometry. For the case of laminar secondary flow, the theory presented in §2 furnishes a number of quantitative predictions that can be compared with measurements.

Three sets of experiments were performed. In the first of these, flow visualization was used to describe the flow streamlines near the flat-plate surface and to investigate the onset of secondary flow and turbulence. In the second set of experiments, hot-film heat-transfer probes were used to measure the fluid shear stress at the plate surface. Lastly, experiments were performed to measure the torque required to rotate the cone above the flat plate.

3.1. *Flow visualization*

For the flow-visualization experiments, a Plexiglas cone-and-plate device was constructed. Three interchangeable cones of standard radii 10.8 cm were made. These had cone angles of 1°, 3° and 5° machined to an accuracy of $\pm 0.1^\circ$. Both the cone and flat-plate surfaces were highly polished. A range of cone rotational rates of 0–300 r.p.m. could be produced.

Two sets of flow-visualization experiments were performed. In the first of these, dye streaklines were entrained into the flow near the flat-plate surface in order to visualize the fluid streamlines under various flow conditions. The dye, a water-soluble black ink, was injected by means of a syringe drive, at three individual ports located at $\frac{1}{4}$, $\frac{1}{2}$ and $\frac{3}{4}$ of the plate radius. As the direction of the fluid velocity varies across the cone–plate gap, care was taken to ensure that the dye was entrained by the flow very near the plate surface. Once the syringe drive had brought the dye up to the surface of the plate, the dye was carried along, near the plate surface, by the motion of the fluid. Water and two water–glycerol solutions (48 % and 72 % by weight glycerol) were used to vary the viscosity of the fluid between the cone and plate. The ability to change the fluid viscosity, the cone angle and rotational rate, and the dye-injection position provided a wide range of operating conditions.

In the second sect of flow-visualization experiments, a suspension of fine aluminium flakes (Albron Powder no. 422, Alcoa) in methanol was used to monitor the development of turbulence in the flow. The orientation of the flakes is dependent on the local shear rate of the flow. Hence in turbulent flows a locally changing reflectivity of the suspension is visible. All quantitative flow-visualization data were obtained from photographs recorded with a 35 mm camera located below the flat plate and looking directly up at it.

3.2. *Shear-stress measurements*

Hot-film heat-transfer probes were used to measure the fluid shear stress at the surface of the flat plate. These probes (Model 1237W, Thermo-Systems Inc.) had a sensor element which consisted of a small film of platinum (0.12 × 1.0 mm) coated with a very thin layer of quartz for protection in liquid media. The sensor element and its leads were potted in a stainless-steel tube with an outside diameter of 3.18 mm. The quartz surface coating was polished smooth, and the surface of the probe was aligned to be flush with the surface of the flat plate so as to avoid any local disturbances to the flow. The three port locations that had been used for the dye injection in the flow-visualization experiments were also used to position the sensor element of the hot-film heat-transfer probes at the flat-plate surface.

The relation between heat transfer and shear stress for these probes was established empirically. In order to facilitate simple and accurate calibration, it is useful to find an appropriate non-dimensional form for representing these data.

For the case of a thermal probe embedded in an otherwise-adiabatic wall subjected to a steady laminar flow that possesses a velocity profile that can be considered linear over a distance from the wall larger than the thermal boundary-layer thickness above the probe, the functional relationship between heat transfer and surface shear stress can be expressed (Lévêque 1928) as

$$Nu = 0.807 N_{\mathrm{w}}^{\frac{1}{3}}. \tag{28}$$

Here

$$Nu = \frac{QL}{k(T_{\mathrm{w}} - T_{\infty})}, \quad N_{\mathrm{w}} \equiv Pr \frac{L^2}{\nu}\left(\frac{\partial u}{\partial z}\right)_{\mathrm{w}}, \quad Pr = \frac{c_p \mu}{k}, \tag{29}$$

where Q is the local heat-transfer rate per unit area, L is the length of the hot-film element in the flow direction, k is the fluid thermal conductivity, T_{w} is the local wall temperature, T_{∞} is the freestream fluid temperature, c_p and ν are respectively the specific heat and kinematic viscosity of the fluid, and $(\partial u/\partial z)_{\mathrm{w}}$ denotes the local velocity gradient at the wall.

The average heat-transfer rate $\bar{Q}$ per unit area may be equated to the electrical dissipation in the probe divided by the size of the probe:

$$\bar{Q} = \frac{V^2}{R}\frac{1}{WL}, \tag{30}$$

where V is the voltage across the thin film, R is the film resistance and W is the dimension of the film normal to the direction of the flow.

Incorporating (28)–(30) and including the expression for the wall shear stress $\tau_{\mathrm{w}} = \mu(\partial u/\partial z)_{\mathrm{w}}$, an expression is obtained relating the voltage drop V across the thin film directly to the wall shear stress τ_{w}:

$$V^2 = A\tau_{\mathrm{w}}^{\frac{1}{3}}, \tag{31}$$

where A is a constant for any particular fluid, sensor geometry and probe resistance.

The last expression assumes that the only form of heat exchange taking place is from the sensor element directly to the fluid. As the wall in which the sensor element is embedded is not adiabatic, conduction into the substrate is an important contribution to the probe heat loss. A suitable calibration relation has been found to be of the form

$$V^2 = A\tau_{\mathrm{w}}^{\frac{1}{3}} + B, \tag{32}$$

where the second term B represents conduction into the substrate. The values A and B represent experimental calibration constants that must be determined for each probe under conditions that approximate those of any proposed measurements. Consequently the hot-film heat-transfer probe was calibrated in position in the flat plate of the cone-and-plate device. The calibration was performed in conditions of primary flow, namely laminar flow with a linear velocity profile between the cone and the plate, for which $\tau_{\mathrm{w}} = \mu\omega/\alpha$. A plot of V^2 as a function of $\tau_{\mathrm{w}}^{\frac{1}{3}}$ gave a straight line with positive slope and intercept. It is possible to apply the same calibration relation (32) to conditions with secondary flow. In this case the total shear stress τ_{w}

on the plate is the vector sum of two components which are designated as $\tau_{r\theta}$ in the azimuthal direction and $\tau_{\theta r}$ in the radial direction. The direction of τ_w is the same as that of the surface streamline; consequently the azimuthal shear stress may be computed from

$$\tau_{r\theta} = \tau_w \cos\phi, \tag{33}$$

where ϕ corresponds to the angle between the azimuthal direction and the dye streakline as measured during the flow-visualization experiments. Prior to each shear-stress measurement, the hot-film-probe sensor element was rotated to an angle that maximized the probe output voltage, indicating that the sensor element was indeed aligned perpendicular to the direction of flow. For local values of $\tilde{R}$ less than 1, this angle approximated that given by the theoretical relation

$$\phi = \tan^{-1}[-0.8\tilde{R} + O(\tilde{R}^3)]. \tag{25}$$

The probe output was not particularly sensitive to angle, being nearly at the maximum output over a 5° band. Shear-stress measurements were made under a variety of operating conditions and are described in §4.2.

3.3. *Torque measurements*

In this set of experiments, the torque required to rotate the cone above the flat plate was measured using a Brookfield cone–plate viscometer (Model LVT). This device incorporated an accurate torque indicator. A wide range of operating conditions was achieved with the use of two interchangeable cones ($\alpha = 1.57°$ and $3.00°$), three fluids with differing kinematic viscosities ν (methanol, 0.68×10^{-2} cm^2/s; water 1.0×10^{-2} cm^2/s; and silicone oil, 20×10^{-2} cm^2/s), and varying cone rotational rates (0–300 r.p.m.). The cone radius R_0 was 33 mm in all instances. $\tilde{R}_0$ is defined to be the value of $\tilde{R}$ evaluated using the cone radius R_0. The possibility of varying the cone rotational rate as well as the cone angle and fluid kinematic viscosity gave a wide range of operating conditions in terms of the $\tilde{R}_0$ values attained. It was possible moreover to obtain measurements at identical values of $\tilde{R}_0$ using different combinations of the contributing physical variables ν, α and ω.

The torque T required to rotate the cone above the flat plate is simply the integral of the azimuthal component of the shear stress across the entire cone surface, from $r = 0$ to $r = R_0$:

$$T = \int_0^{R_0} \tau_{r\theta} 2\pi r^2 \, \mathrm{d}r, \tag{34}$$

where $\tau_{r\theta}$ is the local shear stress at each point on the cone surface. A dimensionless shear stress may be defined as

$$\tau^*_{r\theta} = \frac{\tau_{r\theta}}{\mu\omega/\alpha} \equiv 1 + g(\tilde{R}), \tag{35}$$

where the shear stress in primary flow $\tau_p \equiv \mu\omega/\alpha$ is used to non-dimensionalize the shear stress. The definition of the term $g(\tilde{R})$ is predicated on the assumption that the local shear stress on the cone at any radius is only a function of the single parameter $\tilde{R}$. This is a prediction of the theory (27) for small values of $\tilde{R}$; it remains a postulate for large values of $\tilde{R}$, including turbulent flow. For $g(\tilde{R}) \to 0$, $\tau^*_{r\theta} = 1$ and the flow is purely primary. Substituting (35) into (34), the torque may be expressed in terms of the function $g(\tilde{R})$:

$$T = \int_0^{R_0} \frac{\mu\omega}{\alpha} (1 + g(\tilde{R})) \, 2\pi r^2 \, \mathrm{d}r. \tag{36}$$

Using (36) it is possible to express the function $g(\tilde{R})$ in terms of $\tilde{R}$ and experimentally determined torque measurements; this is described below.

The definition of $\tilde{R}$ was established in §2 as

$$\tilde{R} \equiv \frac{r^2 \omega \alpha^2}{12\nu}.$$

Thus, for a fixed geometry, rotational rate and fluid, the radius r may be expressed as

$$r = \tilde{R}^{\frac{1}{2}} \left(\frac{12\nu}{\omega\alpha^2}\right)^{\frac{1}{2}}, \tag{37}$$

$$\mathrm{d}r = \tfrac{1}{2}\tilde{R}^{-\frac{1}{2}} \left(\frac{12\nu}{\omega\alpha^2}\right)^{\frac{1}{2}} \mathrm{d}\tilde{R}. \tag{38}$$

Using (37) and (38), the torque (36) may be expressed as

$$T = \frac{12\pi\mu\nu}{\alpha^3} DL\left(\frac{12\nu}{\omega\alpha^2}\right)^{\frac{1}{2}} \int_0^{\tilde{R}_0} [1+g(\tilde{R})]\, \tilde{R}^{\frac{1}{2}}\, \mathrm{d}\tilde{R}, \tag{39}$$

where

$$\tilde{R}_0 \equiv \frac{R_0^2\, \omega\alpha^2}{12\nu}.$$

If (39) is integrated under conditions where no secondary flow exists (i.e. in the limit of $g(\tilde{R}) \rightarrow 0$) the result is

$$T_{\tilde{R}\rightarrow 0} \equiv T_{\mathrm{p}} = \frac{\mu\omega}{\alpha}\frac{2\pi}{3} R_0^3. \tag{40}$$

This result can be used to normalize the expression for the torque given by (39):

$$\frac{T}{T_{\mathrm{p}}} = 1 + \tfrac{3}{2}\tilde{R}_0^{-\frac{3}{2}} \int_0^{\tilde{R}_0} g(\tilde{R})\, \tilde{R}^{\frac{1}{2}}\, \mathrm{d}\tilde{R}. \tag{41}$$

A new parameter $\tilde{T}$ is now defined such that

$$\tilde{T} \equiv \frac{2}{3}\left(\frac{T}{T_{\mathrm{p}}} - 1\right) \tilde{R}_0^{\frac{3}{2}} = \int_0^{\tilde{R}_0} g(\tilde{R})\, \tilde{R}^{\frac{1}{2}}\, \mathrm{d}\tilde{R}. \tag{42}$$

By differentiating (42) an expression relating $g(\tilde{R})$ and $\tilde{T}$ results

$$[g(\tilde{R})]_{\tilde{R}=\tilde{R}_0} = \frac{1}{\tilde{R}_0^{\frac{1}{2}}} \frac{\mathrm{d}\tilde{T}}{\mathrm{d}\tilde{R}_0}. \tag{43}$$

This expression provides a means whereby the function $g(\tilde{R})$ can be measured experimentally. Measurements of the torque T can be used to determine $\tilde{T}(\tilde{R}_0)$ using the values of T, T_{p} and $\tilde{R}_0$ as they appear in (42). Differentiation of the experimental relation $\tilde{T}(\tilde{R}_0)$ allows computation of $g(\tilde{R}_0)$ using (43). It is not always accurate to differentiate an experimentally determined function, particularly if there is much scatter in the data. There was, however, very little scatter in the torque measurements, as may be seen from the normalized torque values plotted in figure 9.

The method adopted here to determine $g(\tilde{R})$ experimentally rests upon a number of assumptions.First it is implicit that there is only a *single* correlating parameter $\tilde{R}$ that determines the degree of departure from primary flow. Although this is predicted by laminar theory, the success of this correlation in turbulent flow is a conjecture until tested experimentally. A second important assumption is that end effects do not alter the determination of $g(\tilde{R})$ according to (43). In that context it is the *change* of the total torque $\tilde{T}$ with $\tilde{R}_0$ that is the determining factor. Errors from this source would be minimized by small cone angles, as it would be expected that the influence of the end effects would extend into the interior flow between the cone and plate only one or two times the gap height at the cone edge. Further consideration will be given to this question in discussing the experimental results.

4. Results and discussion

4.1. *Flow visualization*

The two forces acting on the fluid in the cone-and-plate device are the centrifugal force, caused by the circular motion of the fluid, and the viscous force, arising from the relative motion between the cone and the plate. It is the relative magnitude of these two forces that govern the motion and this is reflected in the parameter $\tilde{R}$. As $\tilde{R} \rightarrow 0$ the centrifugal force becomes negligible and the fluid streamlines, as marked by the dye streaklines, are concentric circles about the cone apex. This type of motion has been termed primary flow. As the value of $\tilde{R}$ increases, so does the centrifugal force; dye streaklines at the stationary plate surface are oriented towards the centre of the plate; this non-circular motion is termed *secondary flow*. An example of a dye streakline indicating the presence of secondary flow is given in figure 3.

In order to quantify the motion of the streamlines with changing values of $\tilde{R}$, the angle ϕ made by the tangent to the dye streakline at the point of injection and the azimuthal direction (figure 4) was plotted as a function of $\tilde{R}$. The results for a 1° cone angle are shown in figure 5. The theoretical solution for small $\tilde{R}$,

$$\phi = \tan^{-1}[-0.8\tilde{R}+O(\tilde{R}^3)], \tag{25}$$

is indicated by the solid line in this figure. For values of $\tilde{R} \lesssim 0.5$ there is very good agreement between the theoretical solution and the experimental results. Similar results were obtained using cone angles of 3° and 5°. There was, however, some additional scatter for data recorded at the larger cone angles. The method whereby the dye was entrained into the gap along the flat-plate surface by the motion of the fluid was least successful in the case of large cone angles, and the additional scatter was attributed to this fact.

For $\tilde{R} > 4$ the transition to turbulent flow was observed by the breakup of the dye streakline, and an example is given in figure 6. For any given rotational rate, cone angle and fluid viscosity, the value of $\tilde{R}$ increases with increasing radial position from the centre of the flat plate outwards. Thus the first signs of transition to turbulent flow appear at the outer radius of the plate. The turbulence then propagates inwards towards the centre of the plate as the value of $\tilde{R}$ at a fixed radius increases with increasing cone rotational rates. Four photographs, taken during the aluminium-particle flow-visualization experiment, are presented in figure 7 and show the progress of the turbulent front towards the centre of the plate with increasing values of $\tilde{R}_0$. It is interesting to note that any fluid particle near the flat-plate surface will eventually be carried inwards toward the centre of the plate and then outwards along the surface of the cone because of the action of the secondary flow. When $\tilde{R}_0 \gg 1$ and turbulence is present a fluid particle near the outer edge of the plate surface will travel from a region of turbulence into a region of relaminarized flow. The radius of the sharp visual front revealed by the aluminium flakes at the turbulent-to-laminar transition was used to calculate values of $\tilde{R}_{\text{transition}}$ for different flow conditions with $\tilde{R}_0$ at the outer radius of the plate in the range of $4 \gtrsim \tilde{R}_0 \gtrsim 40$. A mean value of $\tilde{R}_{\text{transition}} = 4.0 \pm 0.4$ was found. The turbulence, as made visible by the suspended aluminium flakes in figure 7, bears a striking resemblance to the analogous visualization of a turbulent

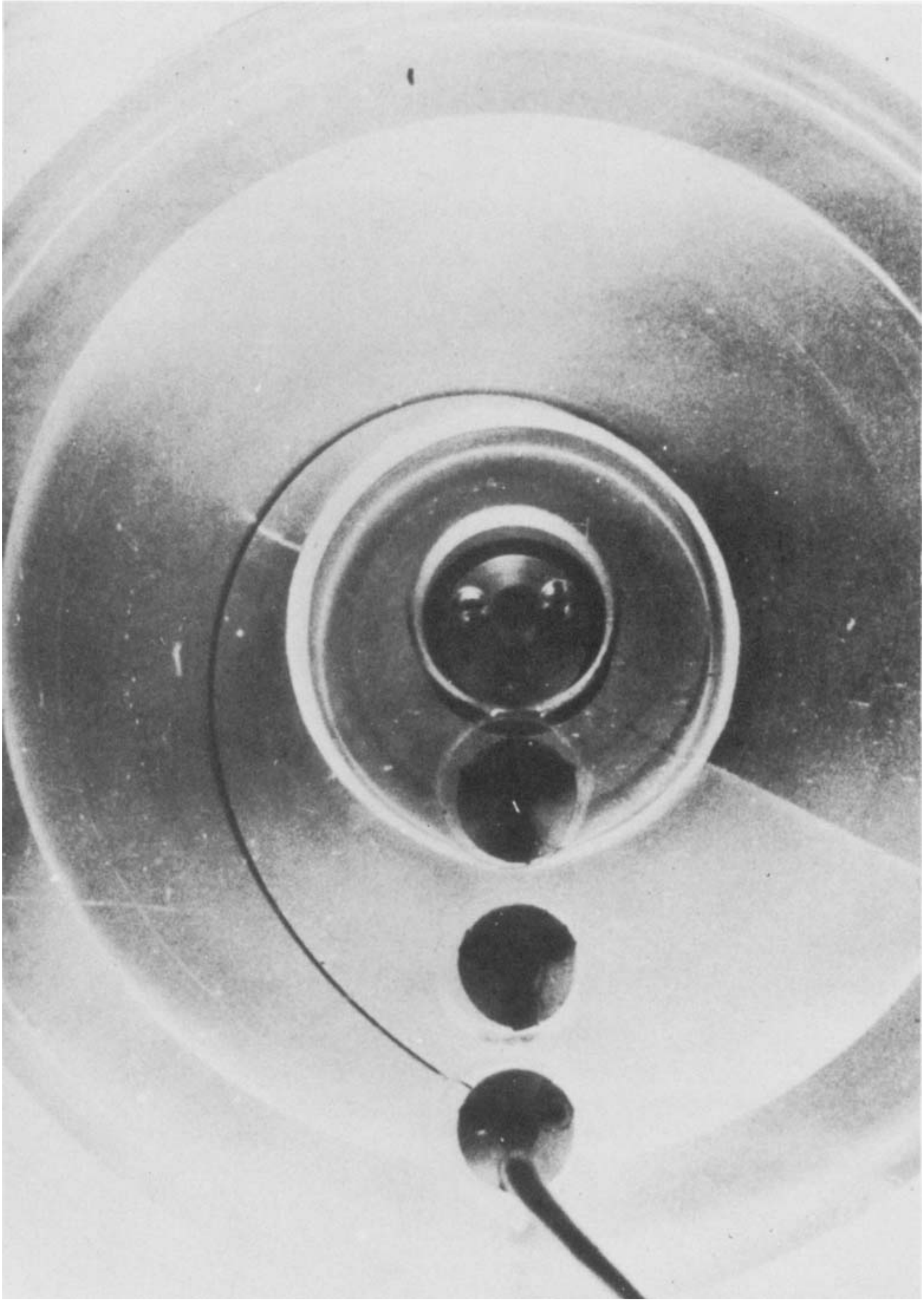

FIGURE 3. Photograph of a dye streakline near the plate surface in secondary flow, $\tilde{R} = 0.8$.

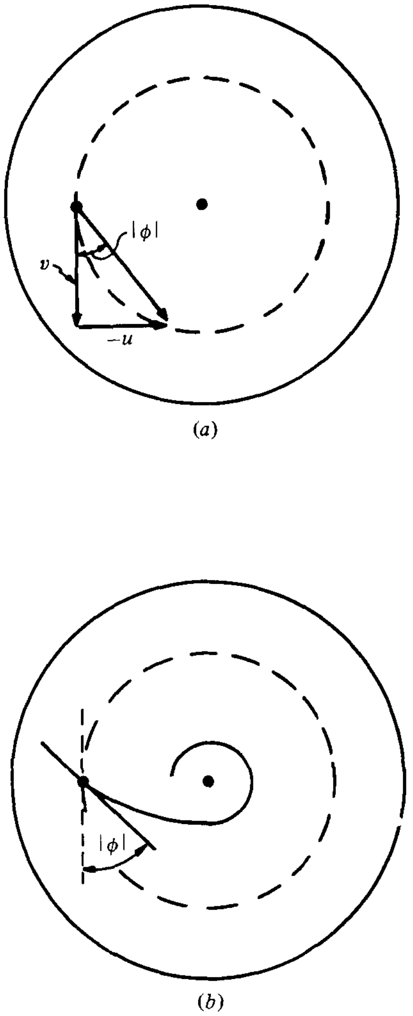

(*a*)

(*b*)

FIGURE 4. (*a*) Azimuthal (v) and radial (u) components of velocity near the plate surface, showing the angle ϕ. (*b*) Schematic representation of a surface streamline. The angle is formed between the azimuthal and the surface directions.

boundary layer reported by Cantwell (1981), although Cantwell's pictures exhibit more orientation of the structure in the streamwise direction than do the pictures included here.

4.2. *Shear-stress measurements*

The experimentally determined azimuthal shear-stress values $\tau_{r\theta}$ are compared with the numerical calculations of Fewell & Hellums (1977)† and the laminar theory for $\tilde{R} \ll 1$, as presented in §2, in figure 8. The azimuthal shear stress has been normalized with the primary-flow shear stress $\tau_{\mathrm{p}} = \mu\omega/\alpha$. As the calculations of Fewell & Hellums were performed for different cone-edge conditions than those of the current experimental work, their results have only been plotted for values of $\tilde{R}$ corresponding to radial locations within $\frac{3}{4}R_0$, which was the outermost radius of our experimental

---

† The local values of $\tau_{r\theta}$ from Fewell & Hellums on the cone and plate surfaces were obtained by taking the slopes of their theoretical velocity profiles at the surfaces of the cone and plate at different radii from the cone axis and computing the corresponding local values of $\tilde{R}$ from their two parameters which are equivalent to $\tilde{R}_0/\alpha^2$ and α.

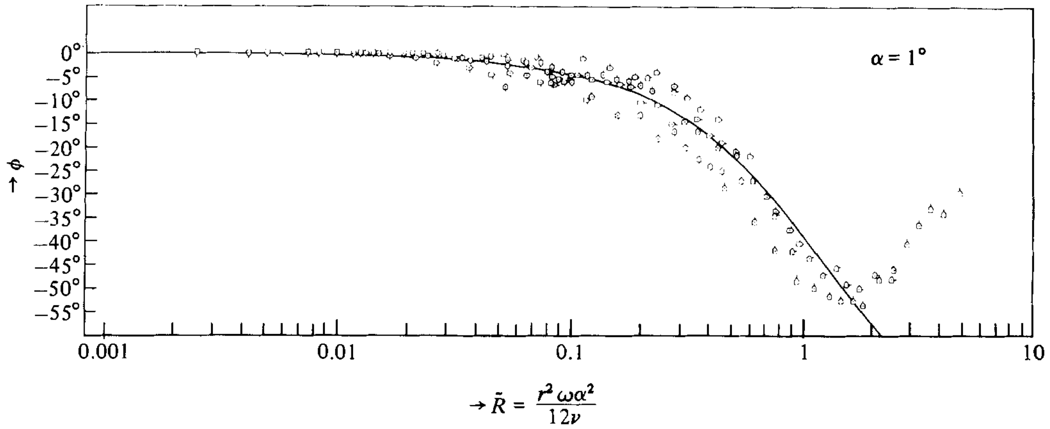

FIGURE 5. Plate-surface dye-streakline direction ϕ as a function of $\tilde{R}$ for a 1° cone.

measurements. For $\tilde{R} \lesssim 0.5$ there is good agreement between the experimental data, the numerical calculations of Fewell & Hellums and our laminar theory based on an expansion of the equations of motion for small $\tilde{R}$. Shear-stress measurements were obtained for the surface of the cone from a series of torque measurements as described in the following section. These data have also been plotted (solid line) in figure 8 and are found to be in excellent agreement with the laminar theory and the numerical calculations of Fewell & Hellums for $\tilde{R} < 0.5$.

4.3. *Torque measurements*

Torque data obtained from the Brookfield cone–plate viscometer and normalized with respect to the torque (40) in primary flow have been plotted as a function of $\tilde{R}_0$ in figure 9. The empirical curve

$$\frac{T}{T_{\mathrm{p}}} = 1 + 1.290\frac{\tilde{R}_0^{\frac{3}{2}}}{3.5+\tilde{R}_0} \tag{44}$$

has been fitted to these data and is indicated by the broken line in this figure. The torque data obtained by Cheng (1968) for 1°, 2° and 4° cones have been replotted in terms of the single parameter $\tilde{R}_0$ in figure 10. For $\tilde{R}_0 \gtrsim 1$ there is good agreement between these data and the empirical expression (44) for the normalized torque which is plotted as a solid line in the figure. The numerical calculations of total cone torque by Fewell & Hellums (1977) are compared with the normalized torque expression (44) in figure 11. In this case the calculations of Fewell & Hellums show a smaller increase in torque than is reported in this paper. Their calculations agree more closely with Cheng's data. In each instance, both the theory and the experiments appear to be adequately represented by the single parameter $\tilde{R}$.

Substituting (44) and (42) into (43), the following expression is obtained for $g(\tilde{R}_0)$:

$$g(\tilde{R}_0) = 2.58\frac{\tilde{R}_0^{\frac{3}{2}}}{3.5+\tilde{R}_0} - 0.86\frac{\tilde{R}_0^{\frac{5}{2}}}{(3.5+\tilde{R}_0)^2}. \tag{45}$$

Thus the normalized shear stress on the surface of the cone may be expressed, using (35), as

$$\tau^*_{r\theta} = 1 + 2.58\frac{\tilde{R}_0^{\frac{3}{2}}}{3.5+\tilde{R}_0} - 0.86\frac{\tilde{R}_0^{\frac{5}{2}}}{(3.5+\tilde{R}_0)^2}. \tag{46}$$

The result is plotted in figure 8 and labelled $1+g(\tilde{R})$. It is important to note that the shear-stress component $\tau_{r\theta}$ on the cone surface is always greater than the value

FIGURE 6. Photograph of dye streakline near plate surface in turbulent flow, $\tilde{R} = 16.9$.

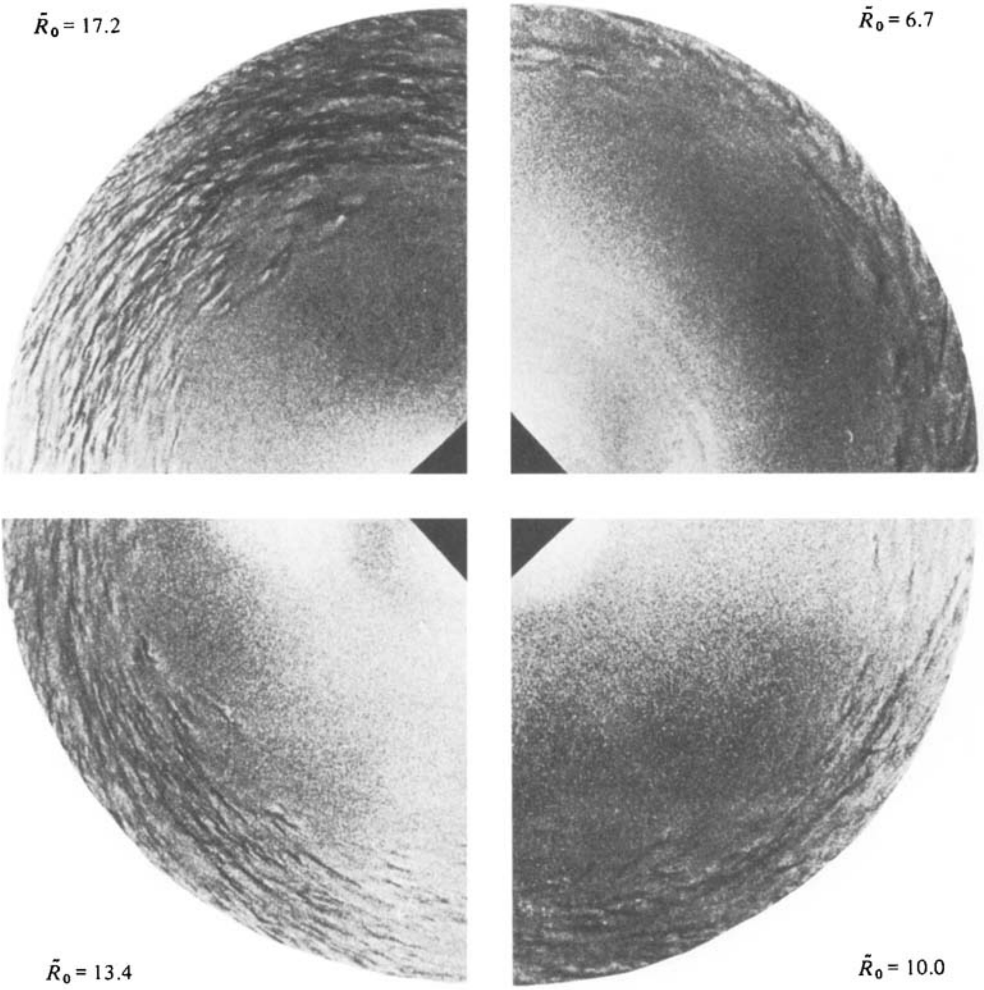

FIGURE 7. Four photographs taken during aluminium-particle flow-visualization experiment showing progress of turbulent front with increasing values of $\tilde{R}_0$, and the cone rotating counterclockwise.

for primary flow; conversely the plate shear-stress component $\tau_{r\theta}$ is less than the primary-flow value prior to the onset of turbulence.†

4.4. *Velocity profiles*

The laminar theory presented in §2 predicts that there will be an increasing distortion of the azimuthal velocity profile with increasing values of $\tilde{R}$. No direct measurements of the azimuthal velocity profile were made during the present investigation; however, it was possible to compare the predictions of laminar theory with the numerical calculations of Fewell & Hellums (1977).

For the present theory, the azimuthal velocity is expressed for small $\tilde{R}$ as

$$v = \omega r(\tilde{v}_0 + \tilde{R}^2\tilde{v}_2 + \ldots),$$

---

† Note that the *total* shear stress, as experienced by a test specimen on the plate, for example, is $\tau_{r\theta}/\cos\phi$, where ϕ is the angle of the total shear-stress vector with respect to the azimuthal direction.

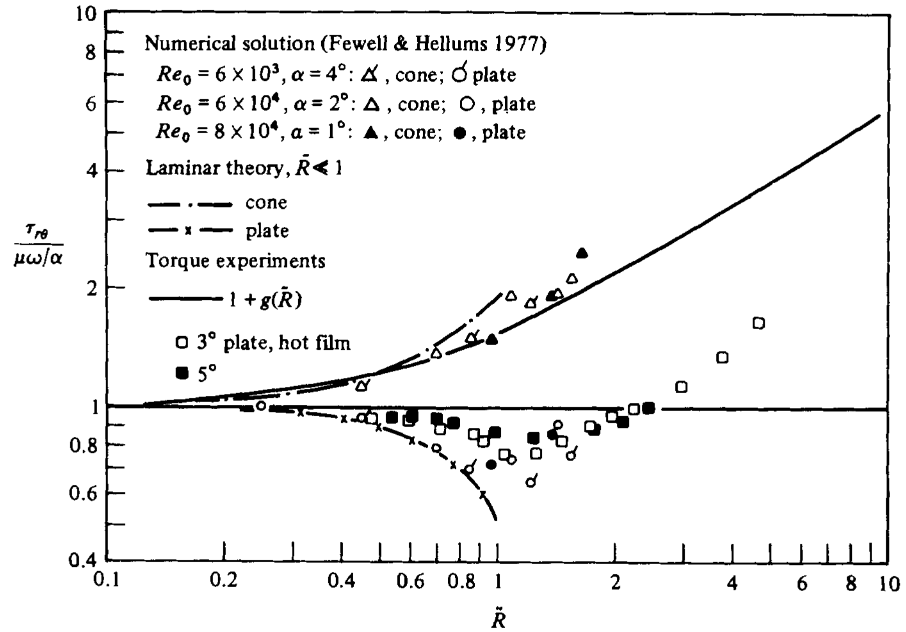

FIGURE 8. Normalized azimuthal component of shear stress $\tau_{r\theta}/(\mu\omega/\alpha)$ on the cone and plate surfaces. Comparison between the laminar theory, the numerical solutions of Fewell & Hellums (1977), and the experimental measurements reported in this paper.

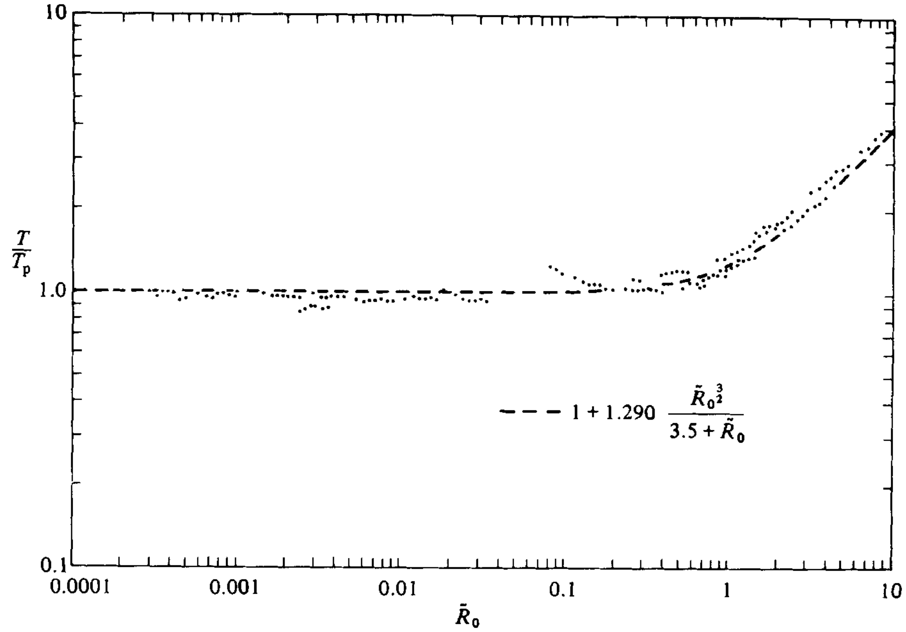

FIGURE 9. Normalized torque required to rotate cone above a flat plate. Data taken with Brookfield viscometer. Broken line represent an analytic fit, and $\tilde{R}_0$ is the parameter $\tilde{R}$ evaluated at the cone outer radius.

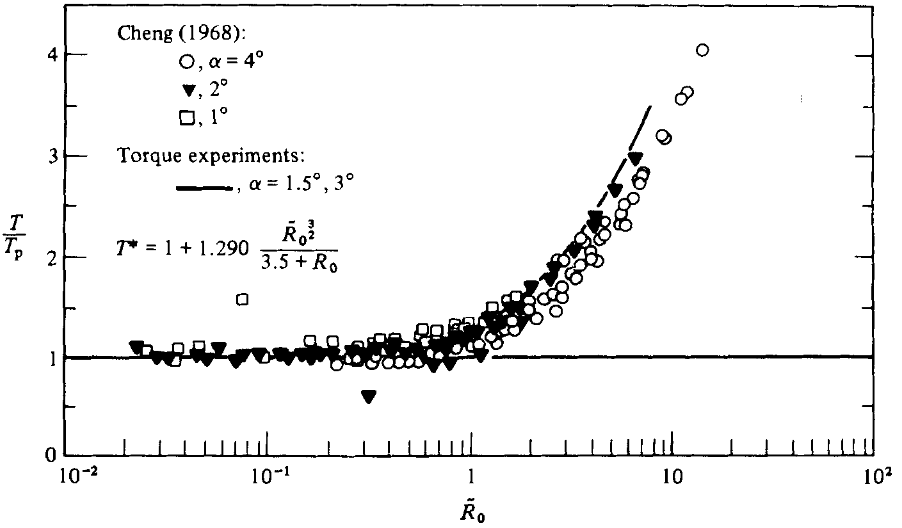

FIGURE 10. Comparison between the normalized torque data of Cheng (1968) and the analytic fit obtained from present experiments as shown in figure 9.

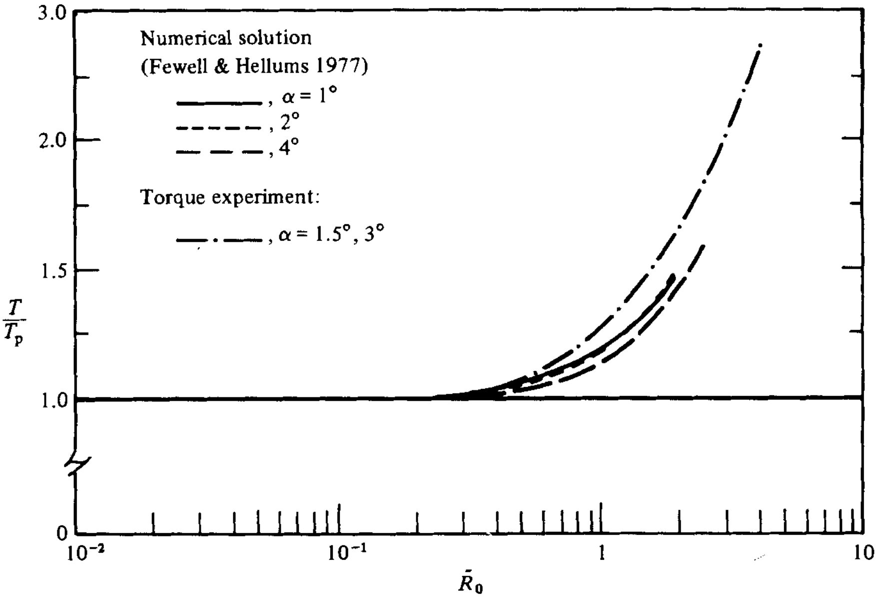

FIGURE 11. Comparison between the normalized torque computed from the numerical calculations of Fewell & Hellums (1977) and an analytic fit to the present experiments as shown in figure 9.

where $\tilde{v}_0$ is the non-dimensional velocity component (20) in primary flow, and $\tilde{R}^2\tilde{v}_2$ is the correction (23) for the deviation of the azimuthal velocity beyond primary flow. The corresponding velocity correction from Fewell & Hellums (1977) is the *difference* between their computed velocity profile and a linear profile (primary flow) between the plate and the cone surface.[†]

The present predictions of azimuthal velocity distortion are compared with the corresponding results from Fewell & Hellums in figure 12. For $\tilde{R} = 0.44$ there is good agreement between the present analytic prediction and the numerical solution. In

---

[†] As it was difficult to take differences between the plotted profiles in Fewell & Hellums and straight lines, the original figures in Fewell's Ph.D. thesis were used (see Fewell 1974).

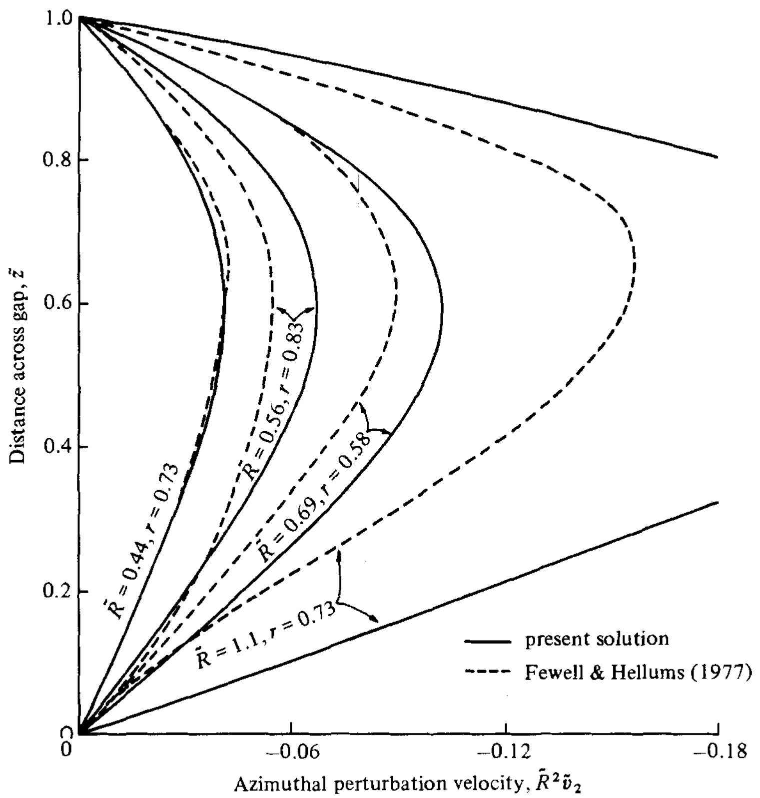

FIGURE 12. Comparison between the normalized second-order azimuthal-velocity correction term and correction to a linear velocity profile (primary flow) as computed by Fewell & Hellums (1977).

this case the numerical calculations were performed at 73 % of the cone outer radius, where end effects should not be important. Agreement is fair for the two pairs of curves at $\tilde{R} = 0.56$ and $\tilde{R} = 0.69$. The maximum values of the distortion in these two cases agree to about 15 %, and the slopes (shear-stress increments) at the cone and plate are even more accurately predicted (to within about 10 %). As $\tilde{R}$ approaches unity, however, the present analytic method based on an expansion for small $\tilde{R}$ fails to be quantitatively accurate.

The shear-stress component $\tau_{r\theta}$ on the cone is computed from the gradient of the azimuthal velocity. It is evident from the data presented in figure 12 that the shear stress on the cone is larger than that on the plate at any interior radius away from the cone edge. The velocity perturbation $\tilde{R}^2\tilde{v}_2$ is negative everywhere in the fluid space; therefore the velocity gradient and surface shear stress is *less* than primary flow at the plate and *more* than primary flow at the cone.

5. Conclusions

An analytic description of the flow in a cone-and-plate geometry has been developed by performing an asymptotic expansion of the Navier–Stokes equations. The single parameter of the expansion is $\tilde{R} = r^2\omega\alpha/12\nu$. The analytic flow description appears to be accurate for small cone angles, for the portion of the flow field that is away from the periphery of the cone, and for values of $\tilde{R}$ less than about 0.5. The fluid shear stress, the angle of the plate-surface streamlines, and the onset of turbulence as observed using flow-visualization continue to be describable as functions of the single variable $\tilde{R}$ with increasing values of $\tilde{R}$. The fact that this entire range of flow phenomena may be described by a single parameter allows a very succinct and compact description of the fluid motion in this device.

The present results do not attempt to describe the flow near the outer rim of the cone, where edge effects and the precise boundary conditions are very important. Fewell & Hellums (1977) calculated the behaviour of the flow in this region for the case of a free-surface termination to the fluid. There are changes in the shear stresses on the cone and plate near their outer edges that serve to equalize the torques on the cone and plate. In contrast to the procedure of Turian (1972), Fewell & Hellums did not require any assumptions to achieve the required torque balance. Within the interior of the fluid space, the azimuthal shear stress $\tau_{r\theta}$ depends only on the single parameter $\tilde{R}$. In primary flow, i.e. for $\tilde{R} \rightarrow 0$, $\tau_{r\theta}$ is the same on the cone and the plate at any given radius. As $\tilde{R}$ increases, $\tau_{r\theta}$ departs from its primary value; the cone shear stress becomes more than, and the plate shear stress becomes less than, the primary value. The quantitative predictions of the laminar theory are in good agreement with the present shear-stress measurements for $\tilde{R} \lesssim 0.5$.

It was not possible to measure the fluid shear stress on the cone directly. Rather, the torque required to rotate the cone was measured and the resulting data were differentiated to obtain the shear stress on the cone surface. This method is not without difficulty. A major assumption is that the shear stress throughout the device may be characterized by the single parameter $\tilde{R}$. This assumption, however, fails near the outer edge of the device where the end conditions are important. The accuracy of the measured shear stress is not compromised unless the *derivative* of the torque is affected. The results that are reported in figure 8 suggest that the procedure is in quantitative agreement not only with the present theory and that of Fewell & Hellums (1977)† but also with the data of Cheng (1968).

Turbulence appears within the fluid space for all radii associated with a local value of $\tilde{R}$ greater than 4. The fact that a single value of the parameter $\tilde{R}$ correlates the onset of turbulence for a variety of cone angles, radii, viscosities and rotational velocities suggests that the turbulence is triggered by an instability associated with the distorted velocity profile produced by the secondary flow. To date there have been no detailed measurements of the velocity-fluctuation spectrum in the turbulent region; photographs taken of suspended aluminium flakes, however, suggest that the turbulence does not contain any prominent discrete frequencies. The disturbance patterns in the aluminium flakes had structures that were extended in the flow direction in a manner similar to that observed by Cantwell (1981) at the base of a turbulent boundary layer.

One of the interesting features of this geometry is the relaminarization of the flow near the plate surface. The secondary motion sustained by centrifugal force circulates fluid outward near the cone surface and inward near the plate surface. Streamlines are deviated inward from the azimuthal direction by approximately 45° at the plate surface for values of $\tilde{R}$ exceeding unity. Fluid near the cone will therefore travel from the inner part of the device, where $\tilde{R} < 1$, into a region where $\tilde{R} > 4$ and the flow is turbulent. Conversely, fluid near the plate will move from a region of turbulence to a region where the flow is essentially laminar. This 'relaminarization' is an intriguing phenomenon and deserves further study. There are only a few instances in which relaminarization has been observed (see e.g. Coles & Van Atta 1967;

---

† The points on figure 8 from Fewell & Hellums are obtained from the slopes of the velocity profiles that they computed and represent radial positions away from the outer edge of the cone.

Narasimha & Sreenivasan 1973; Wygnanski & Champaigne 1973; Wygnanski, Sokolov & Friedman 1975). It is evident in figure 7 that the turbulent front is very sharp and that the fluid goes from gross manifestations of turbulence to essentially laminar flow in a distance in the flow direction of a few gap heights.

The cone-and-plate flow was investigated for the purpose of assessing the influence of fluid shear stress on living biological samples. One attractive feature of the cone-and-plane geometry is the possibility of producing both laminar and turbulent flow with the same time-mean shear stress in a single device. Using (33), (35) may be rewritten for the plate surface as

$$\tau_{r\theta} = \frac{\mu\omega}{\alpha}\frac{1+k(\tilde{R})}{\cos\phi}, \tag{47}$$

or, dividing both sides by $\tilde{R}$,

$$\frac{\tilde{R}\cos\phi}{1+k(\tilde{R})} = \frac{\rho r^2\omega^2\alpha}{12\tau_{r\theta}}. \tag{48}$$

The term $k(\tilde{R})$ measures the decrease of the plate shear-stress component $\tau_{r\theta}$ below the value for primary flow, and is defined as the departure from unity of $\tau_{r\theta}/(\mu\omega/\alpha)$ on the plate, as illustrated in figure 8.

The angle ϕ is a smoothly varying function of r as defined by figure 5. The left-hand side of (48) is therefore a smoothly varying single-valued function of $\tilde{R}$ whose value is strictly equal to $\tilde{R}$ at small values of $\tilde{R}$ and something slightly less than $\tilde{R}$ for larger values of $\tilde{R}$. With the value of $\tau_{r\theta}$ fixed, the value of $\tilde{R}$ can be changed from 0.5 (associated with laminar flow) to 4 (indicative of turbulent flow) by increasing the radius of the observation point by $\sqrt{2}$, increasing the rotational rate by the same factor, doubling the cone angle, and adjusting the fluid viscosity slightly to compensate for the variation of the terms $k(\tilde{R})$ and ϕ. Thus a variety of shear-stress levels can be created with alternative conditions producing either laminar or turbulent flow. This property may prove useful for other fluid-dynamical investigations as well.

This research was supported by the Whitaker Health Services Fund and the National Heart, Lung and Blood Institute (HL 25536, HL 21859).

Appendix. Asymptotic expansion of the equations of motion for cone-and-plate flow

The simplified Navier–Stokes equations (8)–(11) for cone-and-plate flow are repeated below:

$$r\text{-momentum}\quad -\frac{v^2}{r} = -\frac{1}{\rho}\frac{\partial p}{\partial r} + \nu\frac{\partial^2 u}{\partial z^2}, \tag{A 1}$$

$$\theta\text{-momentum}\quad u\frac{\partial v}{\partial r} + \frac{uv}{r} + w\frac{\partial v}{\partial z} = \nu\frac{\partial^2 v}{\partial z^2}, \tag{A 2}$$

$$z\text{-momentum}\quad 0 = -\frac{1}{\rho}\frac{\partial p}{\partial z} + \nu\frac{\partial^2 w}{\partial z^2}, \tag{A 3}$$

$$\text{continuity}\quad \frac{\partial u}{\partial r} + \frac{u}{r} + \frac{\partial w}{\partial z} = 0. \tag{A 4}$$

The boundary conditions of no slip at the cone or plate surface can be expressed as follows (for $\alpha \ll 1$):

$$\left.\begin{aligned} &u = v = w = 0 \quad (z = 0),\\ &u = w = 0, \quad v = r\omega \quad (z = r\alpha).\end{aligned}\right\} \tag{A 5}$$

Before solving the equations of motion, the following transformation of variables is performed:

$$\tilde{v} = \frac{v}{\omega r}, \quad \tilde{u} = \frac{u}{\omega r}, \quad \tilde{w} = \frac{w}{\alpha\omega r}, \quad \tilde{z} = \frac{z}{r\alpha}, \quad \tilde{r} = r. \tag{A 6}$$

The three velocity components $\tilde{u}$, $\tilde{v}$, $\tilde{w}$ are assumed to be of the following form:

$$\tilde{u} = (\tilde{u}_0 + \tilde{R}\tilde{u}_1 + \tilde{R}^2\tilde{u}_2 + \ldots), \tag{A 7}$$

$$\tilde{v} = (\tilde{v}_0 + \tilde{R}\tilde{v}_1 + \tilde{R}^2\tilde{v}_2 + \ldots), \tag{A 8}$$

$$\tilde{w} = (\tilde{w}_0 + \tilde{R}\tilde{w}_1 + \tilde{R}^2\tilde{w}_2 + \ldots), \tag{A 9}$$

where the expansion parameter $\tilde{R}$ is defined as

$$\tilde{R} \equiv \frac{r^2\omega\alpha^2}{12\nu}, \tag{A 10}$$

and $\tilde{u}_0, \tilde{u}_1, \ldots, \tilde{v}_0, \ldots, \tilde{w}_0, \ldots$, are normalized components of velocity.

Using these transformed variables, the Navier–Stokes equations (A 1)–(A 4) may be rewritten as

$$r\text{-momentum} \quad \frac{\partial^2\tilde{u}}{\partial\tilde{z}^2} + 12\tilde{R}\tilde{v}^2 - \frac{\tilde{r}\alpha^2}{\mu\omega}\frac{\partial p}{\partial\tilde{r}} = 0, \tag{A 11}$$

$$\theta\text{-momentum} \quad \frac{\partial^2\tilde{v}}{\partial\tilde{z}^2} - 12\tilde{R}\left[2\tilde{u}\tilde{v} + \tilde{r}\tilde{u}\frac{\partial\tilde{v}}{\partial\tilde{r}} + (\tilde{w} - \tilde{u}\tilde{z})\frac{\partial\tilde{v}}{\partial\tilde{z}}\right] = 0, \tag{A 12}$$

$$z\text{-momentum} \quad \frac{\partial^2\tilde{w}}{\partial\tilde{z}^2} - \frac{1}{\mu\omega}\frac{\partial p}{\partial\tilde{z}} = 0, \tag{A 13}$$

$$\text{continuity} \quad \tilde{r}\frac{\partial\tilde{u}}{\partial\tilde{r}} - \tilde{z}\frac{\partial\tilde{u}}{\partial\tilde{z}} + \tilde{u} + \frac{\partial\tilde{w}}{\partial\tilde{z}} = 0. \tag{A 14}$$

The transformed boundary conditions at the cone and plate surface are

$$\left.\begin{aligned} \tilde{u}_0 &= \tilde{u}_1 = \tilde{u}_2 = \ldots = 0, \\ \tilde{v}_0 &= \tilde{v}_1 = \tilde{v}_2 = \ldots = 0, \\ \tilde{w}_0 &= \tilde{w}_1 = \tilde{w}_2 = \ldots = 0 \end{aligned}\right\} \quad (\tilde{z} = 0); \tag{A 15a}$$

$$\left.\begin{aligned} \tilde{u}_0 &= \tilde{u}_1 = \tilde{u}_2 = \ldots = 0, \\ \tilde{w}_0 &= \tilde{w}_1 = \tilde{w}_2 = \ldots = 0, \\ \tilde{v}_0 &= 1, \\ \tilde{v}_1 &= \tilde{v}_2 = \ldots = 0 \end{aligned}\right\} \quad (\tilde{z} = 1). \tag{A 15b}$$

The transformed Navier–Stokes equations may now be solved by the method of asymptotic expansion. The normalized velocity components (A 7)–(A 9) are substituted into (A 11)–(A 14). The terms in each of the resulting equations are then grouped according to their order of magnitude:

$$r\text{-momentum} \quad \left[\frac{\partial^2\tilde{u}_0}{\partial\tilde{z}^2}\right] + \tilde{R}\left[\frac{\partial^2\tilde{u}_1}{\partial\tilde{z}^2} + 12\tilde{v}_0^2 - \frac{12}{\rho\omega^2\tilde{r}}\frac{\partial p}{\partial\tilde{r}}\right] + \tilde{R}^2\left[\frac{\partial^2\tilde{u}_2}{\partial\tilde{z}^2} + 24\tilde{v}_0\tilde{v}_1\right]$$

$$+ \tilde{R}^3[\ldots] + \ldots = 0, \tag{A 16}$$

$$\theta\text{-momentum}\quad \left[\frac{\partial^2\tilde{v}_0}{\partial\tilde{z}^2}\right]+\tilde{R}\left[\frac{\partial^2\tilde{v}_1}{\partial\tilde{z}^2}-24\tilde{u}_0\,\tilde{v}_0-12\tilde{r}\tilde{u}_0\frac{\partial\tilde{v}_0}{\partial\tilde{r}}-12\tilde{w}_0\frac{\partial\tilde{v}_0}{\partial\tilde{z}}+12\tilde{z}\tilde{u}_0\frac{\partial\tilde{v}_0}{\partial\tilde{z}}\right]$$

$$+R^2\left[\frac{\partial^2\tilde{v}_2}{\partial\tilde{z}^2}-24\tilde{u}_0\,\tilde{v}_1-24\tilde{u}_1\,\tilde{v}_0-12\tilde{r}\tilde{u}_0\frac{\partial\tilde{v}_1}{\partial\tilde{r}}-12\tilde{r}\tilde{u}_1\frac{\partial\tilde{v}_0}{\partial\tilde{r}}-12\tilde{w}_0\frac{\partial\tilde{v}_1}{\partial\tilde{z}}\right.$$

$$\left.-12\tilde{w}_1\frac{\partial\tilde{v}_0}{\partial\tilde{z}}+12\tilde{z}\tilde{u}_0\frac{\partial\tilde{v}_1}{\partial\tilde{z}}+12\tilde{z}\tilde{u}_1\frac{\partial\tilde{v}_0}{\partial\tilde{z}}\right]+\tilde{R}^3[\ldots]+\ldots=0, \qquad (\text{A }17)$$

$$z\text{-momentum}\quad \left[\frac{\partial^2\tilde{w}_0}{\partial\tilde{z}^2}-\frac{1}{\mu\omega}\frac{\partial p}{\partial\tilde{z}}\right]+\tilde{R}\left[\frac{\partial^2\tilde{w}_1}{\partial\tilde{z}^2}\right]+\tilde{R}^2\left[\frac{\partial^2\tilde{w}_2}{\partial\tilde{z}^2}\right]+\tilde{R}^3[\ldots]=0, \qquad (\text{A }18)$$

$$\text{continuity}\quad \left[\tilde{r}\frac{\partial\tilde{u}_0}{\partial\tilde{r}}-\tilde{z}\frac{\partial\tilde{u}_0}{\partial\tilde{z}}+2\tilde{u}_0+\frac{\partial\tilde{w}_0}{\partial\tilde{z}}\right]+\tilde{R}\left[\tilde{r}\frac{\partial\tilde{u}_1}{\partial\tilde{r}}-\tilde{z}\frac{\partial\tilde{u}_1}{\partial\tilde{z}}+4\tilde{u}_1+\frac{\partial\tilde{w}_1}{\partial\tilde{z}}\right]$$

$$+\tilde{R}^2\left[\tilde{r}\frac{\partial\tilde{u}_2}{\partial\tilde{r}}-\tilde{z}\frac{\partial\tilde{u}_2}{\partial\tilde{z}}+6\tilde{u}_2+\frac{\partial\tilde{w}_2}{\partial\tilde{z}}\right]+\tilde{R}^3[\ldots]+\ldots=0. \qquad (\text{A }19)$$

Each grouping on the left-hand side of each of (A 16)–(A 19) may be set equal to zero, allowing solutions to be obtained for each of the velocity components. These solutions are now presented.

Zeroth-order solutions: $O(\tilde{R}^0)$

From (A 16)–(A 19) the following zeroth-order equations are formed:

$$\frac{\partial^2\tilde{u}_0}{\partial\tilde{z}^2}=0, \qquad (\text{A }20)$$

$$\frac{\partial^2\tilde{v}_0}{\partial\tilde{z}^2}=0, \qquad (\text{A }21)$$

$$\frac{\partial^2\tilde{w}_0}{\partial\tilde{z}^2}-\frac{1}{\mu\omega}\frac{\partial p}{\partial\tilde{z}}=0, \qquad (\text{A }22)$$

$$\tilde{r}\frac{\partial\tilde{u}_0}{\partial\tilde{r}}-\tilde{z}\frac{\partial\tilde{u}_0}{\partial\tilde{z}}+2\tilde{u}_0+\frac{\partial\tilde{w}_0}{\partial\tilde{z}}=0. \qquad (\text{A }23)$$

The solutions to (A 20)–(A 23) for the boundary conditions (A 15) are

$$\tilde{u}_0=0,\quad \tilde{v}_0=\tilde{z},\quad \tilde{w}_0=0. \qquad (\text{A }24)$$

It should be noted that using $\tilde{w}_0=0$ and (A 22) results in

$$\frac{\partial p}{\partial\tilde{z}}=0,$$

and hence

$$p=p(r). \qquad (\text{A }25)$$

Equation (A 24) and (A 25) describe conditions of *primary flow*.

First-order solution: $O(\tilde{R}^1)$

From (A 16)–(A 19) the following first-order equations are formed after substitution of (A 24) and (A 25):

$$\frac{\partial^2 \tilde{u}_1}{\partial \tilde{z}^2} + 12\tilde{z}^2 - \frac{12}{\rho\omega^2 \tilde{r}} \frac{\mathrm{d}p}{\mathrm{d}\tilde{r}} = 0, \tag{A 26}$$

$$\frac{\partial^2 \tilde{v}_1}{\partial \tilde{z}^2} = 0, \tag{A 27}$$

$$\frac{\partial^2 \tilde{w}_1}{\partial \tilde{z}^2} = 0, \tag{A 28}$$

$$\tilde{r}\frac{\partial \tilde{u}_1}{\partial \tilde{r}} - \tilde{z}\frac{\partial \tilde{u}_1}{\partial \tilde{z}^2} + 4\tilde{u}_1 + \frac{\partial \tilde{w}_1}{\partial \tilde{z}} = 0. \tag{A 29}$$

Integrating (A 26) twice and applying the no-slip boundary condition (A 15) gives

$$\tilde{u}_1 = \tfrac{1}{2}\Psi \tilde{z}^2 - \tilde{z}^4 + C\tilde{z}, \tag{A 30}$$

where

$$\Psi = \frac{12}{\rho\omega^2 \tilde{r}} \frac{\mathrm{d}p}{\mathrm{d}\tilde{r}},$$

and C is a constant of integration which may be evaluated from the continuity equation by noting that the net radial flow integrated across the gap height is zero:

$$\int_{\tilde{z}=0}^{\tilde{z}=1} \tilde{u}_1 \,\mathrm{d}\tilde{z} = 0.$$

The boundary and continuity conditions together give $\Psi = 3.6$ and $C = -0.8$. Thus the first-order radial velocity (A 30) may finally be written

$$\tilde{u}_1 = 1.8\tilde{z}^2 - \tilde{z}^4 - 0.8\tilde{z}. \tag{A 31}$$

This non-dimensional radial velocity profile is of order unity and has been plotted in figure 2. The choice of the factor of 12 in the definition (A 10) of $\tilde{R}$ enables the ratio of the secondary to primary flows to be expressed as

$$\frac{\tilde{u}_1}{\tilde{v}_0} = \tilde{R}(1.8\tilde{z} - \tilde{z}^3 - 0.8). \tag{A 32}$$

As the bracketed expression in (A 32) is of order unity, $\tilde{R}$ is a true measure of the degree of secondary flow.

From (A 27) and boundary conditions (A 15) the normalized first-order azimuthal component of velocity $\tilde{v}_1$ is found to be identically equal to zero.

The first-order vertical velocity component $\tilde{w}_1$ may be obtained by substituting the expression (A 31) for $\tilde{u}_1$ into the first-order continuity equation (A 29). After simplification, (A 29) becomes

$$\frac{\partial \tilde{w}_1}{\partial \tilde{z}} = -3.6\tilde{z}^2 + 2.4\tilde{z}. \tag{A 33}$$

Integrating (A 33) with the boundary condition (A 15) gives the following expression for $\tilde{w}_1$:

$$\tilde{w}_1 = 1.2(\tilde{z}^2 - \tilde{z}^3). \tag{A 34}$$

Second-order solution: $O(\tilde{R}^2)$

From (A 16)–(A 19), after substitution of the zeroth-order velocity components (A 24), and noting that the first-order azimuthal velocity component $\tilde{v}_1$ is equal to zero, the following second-order equations are formed:

$$\frac{\partial^2 \tilde{u}_2}{\partial \tilde{z}^2} = 0, \tag{A 35}$$

$$\frac{\partial^2 \tilde{v}_2}{\partial \tilde{z}^2} - 24\tilde{u}_1 \tilde{v}_0 - 12\tilde{w}_1 \frac{\partial \tilde{v}_0}{\partial \tilde{z}} + 12\tilde{z}\tilde{u}_1 \frac{\partial \tilde{v}_0}{\partial \tilde{z}} = 0, \tag{A 36}$$

$$\frac{\partial^2 \tilde{w}_2}{\partial \tilde{z}^2} = 0, \tag{A 37}$$

$$\tilde{r}\frac{\partial^2 \tilde{u}_2}{\partial \tilde{r}} - \tilde{z}\frac{\partial \tilde{u}_2}{\partial \tilde{z}} + 6\tilde{u}_2 + \frac{\partial \tilde{w}_2}{\partial \tilde{z}} = 0. \tag{A 38}$$

From (A 35), (A 37) and the boundary conditions (A 15) the two terms $\tilde{u}_2$ and $\tilde{w}_2$ are found to be identically equal to zero.

After substituting the first-order components $\tilde{u}_1$, (A 31), and $\tilde{w}_1$, (A 34), into (A 36) and simplifying, the following result is obtained:

$$\frac{\partial^2 \tilde{v}_2}{\partial \tilde{z}^2} = 12(0.4\tilde{z}^2 + 0.6\tilde{z}^3 - \tilde{z}^5). \tag{A 39}$$

Integrating this expression twice and using the boundary conditions (A 15), the following expression is obtained for $\tilde{v}_2$:

$$\tilde{v}_2 = \tfrac{1}{175}(-83\tilde{z} + 70\tilde{z}^4 + 63\tilde{z}^5 - 50\tilde{z}^7). \tag{A 40}$$

REFERENCES

Bussolari, S. R., Dewey, C. F. & Gimbrone, M. A. 1982 An apparatus for subjecting living cells to fluid shear stress. *Rev. Sci. Instrum.* **53**, 1851–1854.

Cantwell, B. J. 1981 Organized motion in turbulent flow. *Ann. Rev. Fluid Mech.* **13**, 457–515.

Cheng, D. C.-H. 1968 The effect of secondary flow on the viscosity measurement using a cone-and-plate viscometer. *Chem. Engng Sci.* **23**, 895–899.

Coleman, B. D., Markovitz, H. & Noll, W. 1966 *Viscometric Flows of Non-Newtonian Fluids.* Springer.

Coles, D. E. & Van Atta, C. W. 1967 Digital experiment in spiral turbulence. *Phys. Fluids Suppl.* **10**, SI120–SI121.

Cox, D. B. 1962 Radial flow in the cone–plate viscometer. *Nature* **193**, 670.

Dewey, C. F., Bussolari, S. R., Gimbrone, M. A. & Davies, P. F. 1981 The dynamic response of vascular endothelial cells to fluid shear stress. *Trans. ASME* K: *J. Biomech. Engng* **103**, 177–185.

Fewell, M. E. 1974 The secondary flow of Newtonian fluids in cone-and-plate viscometers. Ph.D. thesis, Rice University.

Fewell, M. E. & Hellums, J. D. 1977 The secondary flow of Newtonian fluids in cone-and-plate viscometers. *Trans. Soc. Rheol.* **21**, 535–565.

Heuser, G. & Krause, E. 1979 The flow field of Newtonian fluids in cone and plate viscometers with small gap angles. *Rheol. Acta* **18**, 553–564.

King, M. J. & Waters, N. D. 1970 The effect of secondary flows in the use of a rheogoniometer. *Rheol. Acta* **9**, 164–170.

Lévêque, M. A. 1928 Transmission de chaleur par convection. *Ann. des Mines* **13**, 201–299.

Miller, C. E. & Hoppmann, W. H. 1963 Velocity field induced in a liquid by a rotating cone. In *Proc. 4th Intl Congr. on Rheology*, Part 2, pp. 619–635. Interscience.

Mooney, M. & Ewart, R. H. 1934 The conicylindrical viscometer. *Physics* **5**, 350–354.

Narasimha, R. & Sreenivasan, K. R. 1973 Relaminarization in highly accelerated turbulent boundary layers. *J. Fluid Mech.* **61**, 417–447.

Pelech, I. & Shapiro, A. H. 1964 Flexible disk rotating on a gas film next to a wall. *Trans. ASME* E: *J. Appl. Mech.* **31**, 577–584.

Savins, J. G. & Metzner, A. B. 1970 Radial (secondary) flows in rheogoniometric devices. *Rheol. Acta* **9**, 365–373.

Slattery, J. C. 1961 Analysis of the cone–plate viscometer. *J. Coll. Sci.* **16**, 431–437.

Turian, R. M. 1972 Perturbation solution of the steady Newtonian flow in the cone and plate and parallel plate systems. *Ind. Engng Chem. Fundam.* **11**, 361–368.

Walters, K. 1975 *Rheometry*. Wiley.

Walters, K. & Waters, N. D. 1966 Polymer systems, deformation and flow. In *Proc. Brit. Soc. Rheol.* (ed. R. E. Wetton & R. W. Whorlow). Macmillan.

Wygnanski, I. J. & Champagne, F. H. 1973 On transition in a pipe. Part 1. The origin of puffs and slugs and the flow in a turbulent slug. *J. Fluid Mech.* **59**, 281–335.

Wygnanski, I., Sokolov, M. & Friedman, D. 1975 On transition in a pipe. Part 2. The equilibrium puff. *J. Fluid Mech.* **69**, 283, 304.